

Deuteron and antideuteron production in Au+Au collisions at $\sqrt{s_{NN}} = 200$ GeV

S.S. Adler,⁵ S. Afanasiev,¹⁷ C. Aidala,⁵ N.N. Ajitanand,⁴³ Y. Akiba,^{20,38} J. Alexander,⁴³ R. Amirikas,¹² L. Aphecetche,⁴⁵ S.H. Aronson,⁵ R. Auerbeck,⁴⁴ T.C. Awes,³⁵ R. Azmoun,⁴⁴ V. Babintsev,¹⁵ A. Baldisseri,¹⁰ K.N. Barish,⁶ P.D. Barnes,²⁷ B. Bassalleck,³³ S. Bathe,³⁰ S. Batsouli,⁹ V. Baublis,³⁷ A. Bazilevsky,^{39,15} S. Belikov,^{16,15} Y. Berdnikov,⁴⁰ S. Bhagavatula,¹⁶ J.G. Boissevain,²⁷ H. Borel,¹⁰ S. Borenstein,²⁵ M.L. Brooks,²⁷ D.S. Brown,³⁴ N. Bruner,³³ D. Bucher,³⁰ H. Buesching,³⁰ V. Bumazhnov,¹⁵ G. Bunce,^{5,39} J.M. Burward-Hoy,^{26,44} S. Butsyk,⁴⁴ X. Camard,⁴⁵ J.-S. Chai,¹⁸ P. Chand,⁴ W.C. Chang,² S. Chernichenko,¹⁵ C.Y. Chi,⁹ J. Chiba,²⁰ M. Chiu,⁹ I.J. Choi,⁵² J. Choi,¹⁹ R.K. Choudhury,⁴ T. Chujo,⁵ V. Cianciolo,³⁵ Y. Cobigo,¹⁰ B.A. Cole,⁹ P. Constantin,¹⁶ D.G. d'Enterria,⁴⁵ G. David,⁵ H. Delagrange,⁴⁵ A. Denisov,¹⁵ A. Deshpande,³⁹ E.J. Desmond,⁵ O. Dietzsch,⁴¹ O. Drapier,²⁵ A. Drees,⁴⁴ R. du Rietz,²⁹ A. Durum,¹⁵ D. Dutta,⁴ Y.V. Efremenko,³⁵ K. El Chenawi,⁴⁹ A. Enokizono,¹⁴ H. En'yo,^{38,39} S. Esumi,⁴⁸ L. Ewell,⁵ D.E. Fields,^{33,39} F. Fleuret,²⁵ S.L. Fokin,²³ B.D. Fox,³⁹ Z. Fraenkel,⁵¹ J.E. Frantz,⁹ A. Franz,⁵ A.D. Frawley,¹² S.-Y. Fung,⁶ S. Garpman,^{29,*} T.K. Ghosh,⁴⁹ A. Glenn,⁴⁶ G. Gogiberidze,⁴⁶ M. Gonin,²⁵ J. Gosset,¹⁰ Y. Goto,³⁹ R. Granier de Cassagnac,²⁵ N. Grau,¹⁶ S.V. Greene,⁴⁹ M. Grosse Perdekamp,³⁹ W. Guryn,⁵ H.-Å. Gustafsson,²⁹ T. Hachiya,¹⁴ J.S. Haggerty,⁵ H. Hamagaki,⁸ A.G. Hansen,²⁷ E.P. Hartouni,²⁶ M. Harvey,⁵ R. Hayano,⁸ X. He,¹³ M. Heffner,²⁶ T.K. Hemmick,⁴⁴ J.M. Heuser,⁴⁴ M. Hibino,⁵⁰ J.C. Hill,¹⁶ W. Holzmann,⁴³ K. Homma,¹⁴ B. Hong,²² A. Hoover,³⁴ T. Ichihara,^{38,39} V.V. Ikonnikov,²³ K. Imai,^{24,38} D. Isenhower,¹ M. Ishihara,³⁸ M. Issah,⁴³ A. Isupov,¹⁷ B.V. Jacak,⁴⁴ W.Y. Jang,²² Y. Jeong,¹⁹ J. Jia,⁴⁴ O. Jinnouchi,³⁸ B.M. Johnson,⁵ S.C. Johnson,²⁶ K.S. Joo,³¹ D. Jouan,³⁶ S. Kametani,^{8,50} N. Kamihara,^{47,38} J.H. Kang,⁵² S.S. Kapoor,⁴ K. Katou,⁵⁰ S. Kelly,⁹ B. Khachaturov,⁵¹ A. Khanzadeev,³⁷ J. Kikuchi,⁵⁰ D.H. Kim,³¹ D.J. Kim,⁵² D.W. Kim,¹⁹ E. Kim,⁴² G.-B. Kim,²⁵ H.J. Kim,⁵² E. Kistenev,⁵ A. Kiyomichi,⁴⁸ K. Kiyoyama,³² C. Klein-Boesing,³⁰ H. Kobayashi,^{38,39} L. Kochenda,³⁷ V. Kochetkov,¹⁵ D. Koehler,³³ T. Kohama,¹⁴ M. Kopytine,⁴⁴ D. Kotchetkov,⁶ A. Kozlov,⁵¹ P.J. Kroon,⁵ C.H. Kuberg,^{1,27} K. Kurita,³⁹ Y. Kuroki,⁴⁸ M.J. Kweon,²² Y. Kwon,⁵² G.S. Kyle,³⁴ R. Lacey,⁴³ V. Ladygin,¹⁷ J.G. Lajoie,¹⁶ A. Lebedev,^{16,23} S. Leckey,⁴⁴ D.M. Lee,²⁷ S. Lee,¹⁹ M.J. Leitch,²⁷ X.H. Li,⁶ H. Lim,⁴² A. Litvinenko,¹⁷ M.X. Liu,²⁷ Y. Liu,³⁶ C.F. Maguire,⁴⁹ Y.I. Makdisi,⁵ A. Malakhov,¹⁷ V.I. Manko,²³ Y. Mao,^{7,38} G. Martinez,⁴⁵ M.D. Marx,⁴⁴ H. Masui,⁴⁸ F. Matathias,⁴⁴ T. Matsumoto,^{8,50} P.L. McGaughey,²⁷ E. Melnikov,¹⁵ F. Messer,⁴⁴ Y. Miake,⁴⁸ J. Milan,⁴³ T.E. Miller,⁴⁹ A. Milov,^{44,51} S. Mioduszewski,⁵ R.E. Mischke,²⁷ G.C. Mishra,¹³ J.T. Mitchell,⁵ A.K. Mohanty,⁴ D.P. Morrison,⁵ J.M. Moss,²⁷ F. Mühlbacher,⁴⁴ D. Mukhopadhyay,⁵¹ M. Muniruzzaman,⁶ J. Murata,^{38,39} S. Nagamiya,²⁰ J.L. Nagle,⁹ T. Nakamura,¹⁴ B.K. Nandi,⁶ M. Nara,⁴⁸ J. Newby,⁴⁶ P. Nilsson,²⁹ A.S. Nyanin,²³ J. Nystrand,²⁹ E. O'Brien,⁵ C.A. Ogilvie,¹⁶ H. Ohnishi,^{5,38} I.D. Ojha,^{49,3} K. Okada,³⁸ M. Ono,⁴⁸ V. Onuchin,¹⁵ A. Oskarsson,²⁹ I. Otterlund,²⁹ K. Oyama,⁸ K. Ozawa,⁸ D. Pal,⁵¹ A.P.T. Palounek,²⁷ V.S. Pantuev,⁴⁴ V. Papavassiliou,³⁴ J. Park,⁴² A. Parmar,³³ S.F. Pate,³⁴ T. Peitzmann,³⁰ J.-C. Peng,²⁷ V. Peresedov,¹⁷ C. Pinkenburg,⁵ R.P. Pisani,⁵ F. Plasil,³⁵ M.L. Purschke,⁵ A.K. Purwar,⁴⁴ J. Rak,¹⁶ I. Ravinovich,⁵¹ K.F. Read,^{35,46} M. Reuter,⁴⁴ K. Reygers,³⁰ V. Riabov,^{37,40} Y. Riabov,³⁷ G. Roche,²⁸ A. Romana,²⁵ M. Rosati,¹⁶ P. Rosnet,²⁸ S.S. Ryu,⁵² M.E. Sadler,¹ N. Saito,^{38,39} T. Sakaguchi,^{8,50} M. Sakai,³² S. Sakai,⁴⁸ V. Samsonov,³⁷ L. Sanfratello,³³ R. Santo,³⁰ H.D. Sato,^{24,38} S. Sato,^{5,48} S. Sawada,²⁰ Y. Schutz,⁴⁵ V. Semenov,¹⁵ R. Seto,⁶ M.R. Shaw,^{1,27} T.K. Shea,⁵ T.-A. Shibata,^{47,38} K. Shigaki,^{14,20} T. Shiina,²⁷ C.L. Silva,⁴¹ D. Silvermyr,^{27,29} K.S. Sim,²² C.P. Singh,³ V. Singh,³ M. Sivertz,⁵ A. Soldatov,¹⁵ R.A. Soltz,²⁶ W.E. Sondheim,²⁷ S.P. Sorensen,⁴⁶ I.V. Sourikova,⁵ F. Staley,¹⁰ P.W. Stankus,³⁵ E. Stenlund,²⁹ M. Stepanov,³⁴ A. Ster,²¹ S.P. Stoll,⁵ T. Sugitate,¹⁴ J.P. Sullivan,²⁷ E.M. Takagui,⁴¹ A. Taketani,^{38,39} M. Tamai,⁵⁰ K.H. Tanaka,²⁰ Y. Tanaka,³² K. Tanida,³⁸ M.J. Tannenbaum,⁵ P. Tarján,¹¹ J.D. Tepe,^{1,27} T.L. Thomas,³³ J. Tojo,^{24,38} H. Torii,^{24,38} R.S. Towell,¹ I. Tseruya,⁵¹ H. Tsuruoka,⁴⁸ S.K. Tuli,³ H. Tydesjö,²⁹ N. Tyurin,¹⁵ H.W. van Hecke,²⁷ J. Velkovska,^{5,44} M. Velkovsky,⁴⁴ L. Villatte,⁴⁶ A.A. Vinogradov,²³ M.A. Volkov,²³ E. Vznuzdaev,³⁷ X.R. Wang,¹³ Y. Watanabe,^{38,39} S.N. White,⁵ F.K. Wohn,¹⁶ C.L. Woody,⁵ W. Xie,⁶ Y. Yang,⁷ A. Yanovich,¹⁵ S. Yokkaichi,^{38,39} G.R. Young,³⁵ I.E. Yushmanov,²³ W.A. Zajc,^{9,†} C. Zhang,⁹ S. Zhou,⁷ S.J. Zhou,⁵¹ and L. Zolin¹⁷

(PHENIX Collaboration)

¹Abilene Christian University, Abilene, TX 79699, USA

²Institute of Physics, Academia Sinica, Taipei 11529, Taiwan

³Department of Physics, Banaras Hindu University, Varanasi 221005, India

⁴Bhabha Atomic Research Centre, Bombay 400 085, India

⁵Brookhaven National Laboratory, Upton, NY 11973-5000, USA

- ⁶University of California - Riverside, Riverside, CA 92521, USA
⁷China Institute of Atomic Energy (CIAE), Beijing, People's Republic of China
⁸Center for Nuclear Study, Graduate School of Science, University of Tokyo, 7-3-1 Hongo, Bunkyo, Tokyo 113-0033, Japan
⁹Columbia University, New York, NY 10027 and Nevis Laboratories, Irvington, NY 10533, USA
¹⁰Dapnia, CEA Saclay, F-91191, Gif-sur-Yvette, France
¹¹Debrecen University, H-4010 Debrecen, Egyetem tér 1, Hungary
¹²Florida State University, Tallahassee, FL 32306, USA
¹³Georgia State University, Atlanta, GA 30303, USA
¹⁴Hiroshima University, Kagamiyama, Higashi-Hiroshima 739-8526, Japan
¹⁵Institute for High Energy Physics (IHEP), Protvino, Russia
¹⁶Iowa State University, Ames, IA 50011, USA
¹⁷Joint Institute for Nuclear Research, 141980 Dubna, Moscow Region, Russia
¹⁸KAERI, Cyclotron Application Laboratory, Seoul, South Korea
¹⁹Kangnung National University, Kangnung 210-702, South Korea
²⁰KEK, High Energy Accelerator Research Organization, Tsukuba-shi, Ibaraki-ken 305-0801, Japan
²¹KFKI Research Institute for Particle and Nuclear Physics (RMKI), H-1525 Budapest 114, POBox 49, Hungary
²²Korea University, Seoul, 136-701, Korea
²³Russian Research Center "Kurchatov Institute", Moscow, Russia
²⁴Kyoto University, Kyoto 606, Japan
²⁵Laboratoire Leprince-Ringuet, Ecole Polytechnique, CNRS-IN2P3, Route de Saclay, F-91128, Palaiseau, France
²⁶Lawrence Livermore National Laboratory, Livermore, CA 94550, USA
²⁷Los Alamos National Laboratory, Los Alamos, NM 87545, USA
²⁸LPC, Université Blaise Pascal, CNRS-IN2P3, Clermont-Fd, 63177 Aubiere Cedex, France
²⁹Department of Physics, Lund University, Box 118, SE-221 00 Lund, Sweden
³⁰Institut für Kernphysik, University of Muenster, D-48149 Muenster, Germany
³¹Myongji University, Yongin, Kyonggido 449-728, Korea
³²Nagasaki Institute of Applied Science, Nagasaki-shi, Nagasaki 851-0193, Japan
³³University of New Mexico, Albuquerque, NM, USA
³⁴New Mexico State University, Las Cruces, NM 88003, USA
³⁵Oak Ridge National Laboratory, Oak Ridge, TN 37831, USA
³⁶IPN-Orsay, Université Paris Sud, CNRS-IN2P3, BP1, F-91406, Orsay, France
³⁷PNPI, Petersburg Nuclear Physics Institute, Gatchina, Russia
³⁸RIKEN (The Institute of Physical and Chemical Research), Wako, Saitama 351-0198, JAPAN
³⁹RIKEN BNL Research Center, Brookhaven National Laboratory, Upton, NY 11973-5000, USA
⁴⁰St. Petersburg State Technical University, St. Petersburg, Russia
⁴¹Universidade de São Paulo, Instituto de Física, Caixa Postal 66318, São Paulo CEP05315-970, Brazil
⁴²System Electronics Laboratory, Seoul National University, Seoul, South Korea
⁴³Chemistry Department, Stony Brook University, SUNY, Stony Brook, NY 11794-3400, USA
⁴⁴Department of Physics and Astronomy, Stony Brook University, SUNY, Stony Brook, NY 11794, USA
⁴⁵SUBATECH (Ecole des Mines de Nantes, CNRS-IN2P3, Université de Nantes) BP 20722 - 44307, Nantes, France
⁴⁶University of Tennessee, Knoxville, TN 37996, USA
⁴⁷Department of Physics, Tokyo Institute of Technology, Tokyo, 152-8551, Japan
⁴⁸Institute of Physics, University of Tsukuba, Tsukuba, Ibaraki 305, Japan
⁴⁹Vanderbilt University, Nashville, TN 37235, USA
⁵⁰Waseda University, Advanced Research Institute for Science and Engineering, 17 Kikui-cho, Shinjuku-ku, Tokyo 162-0044, Japan
⁵¹Weizmann Institute, Rehovot 76100, Israel
⁵²Yonsei University, IPAP, Seoul 120-749, Korea

(Dated: October 25, 2018)

The production of deuterons and antideuterons in the transverse momentum range $1.1 < p_T < 4.3$ GeV/c at mid-rapidity in Au + Au collisions at $\sqrt{s_{NN}} = 200$ GeV has been studied by the PHENIX experiment at RHIC. A coalescence analysis comparing the deuteron and antideuteron spectra with those of protons and antiprotons, has been performed. The coalescence probability is equal for both deuterons and antideuterons and increases as a function of p_T , which is consistent with an expanding collision zone. Comparing (anti)proton yields: $\bar{p}/p = 0.73 \pm 0.01$, with (anti)deuteron yields: $\bar{d}/d = 0.47 \pm 0.03$, we estimate that $\bar{n}/n = 0.64 \pm 0.04$.

PACS numbers: 25.75.Dw

Keywords: relativistic, heavy ion, collisions, deuteron

Ultrarelativistic heavy ion collisions are used to study the behavior of nuclear matter at extreme conditions of

temperature and density, similar to those that existed in the universe a few microseconds after the Big Bang.

Previous measurements indicate that high particle multiplicities [1] and large \bar{p}/p ratios prevail at the Relativistic Heavy-Ion Collider (RHIC), which is expected for a nearly net baryon free region [2]. As the hot, dense system of particles cools, it expands and the mean free path increases until the particles cease interacting (“freeze-out”). At this point, light nuclei like deuterons and antideuterons (d and \bar{d}) can be formed, with a probability proportional to the product of the phase space densities of their constituent nucleons [3, 4]. Thus, invariant yield of deuterons, compared to the protons [5, 6] from which they coalesce, provides information about the size of the emitting system and its space-time evolution.

PHENIX [7] at RHIC, is a versatile detector designed to study the production of leptons, photons, and hadrons over a wide momentum range. In this Letter, results on d and \bar{d} production in Au+Au interactions at $\sqrt{s_{NN}} = 200$ GeV are presented. For the sake of brevity, in the rest of this Letter, our statements will generally apply to both particles and antiparticles.

The East central tracking spectrometer in the PHENIX detector [5, 7, 8] is used in this analysis. The information from the PHENIX Beam-Beam Counters (BBC) and Zero-Degree Calorimeters (ZDC) is used for triggering and event selection. The BBCs are Čerenkov-counters surrounding the beam pipe in the pseudorapidity interval $3.0 < |\eta| < 3.9$, and provide the start timing signal. The ZDCs are hadronic calorimeters 18 m downstream of the interaction region and detect spectator neutrons in a narrow forward cone. Particle identification in the central rapidity region is achieved by measuring momentum (by drift chamber) and time of flight (by time-of-flight detector). The drift chamber (DC) and two layers of pad chambers (PC) are used for tracking and momentum reconstruction [8]. The time-of-flight detector (TOF) spans the pseudorapidity range $|\eta| < 0.35$ and $\Delta\phi = \pi/4$ azimuthally. The TOF consists of plastic scintillators, with a combined time resolution of ≈ 115 ps. The TOF thus provides identification of d and \bar{d} in the transverse momentum (p_T) range $1.1 < p_T < 4.3$ GeV/ c . For $p_T < 1.1$ GeV/ c , the signal to background ratio suffers due to multiple scattering and energy loss effects.

The dataset for this analysis includes 21.6 million minimum bias events. The minimum bias cross section corresponds to $92.2^{+2.5}_{-3}\%$ of the total inelastic Au+Au cross section (6.9 b) [9]. Using the momentum determined by the DC, which has a resolution of $\delta p/p \approx 0.7\% \oplus 1\% p$ GeV/ c , and the time of flight from the event vertex provided by the TOF, the mass of the particle is determined. The d and \bar{d} yields are obtained by fitting the mass squared distributions to the sum of a Gaussian signal and an exponential background. Examples of mass squared distributions with fits for antideuterons in minimum bias collisions are shown in Fig. 1.

The raw yields are corrected for effects of detector acceptance, reconstruction efficiency and detector occu-

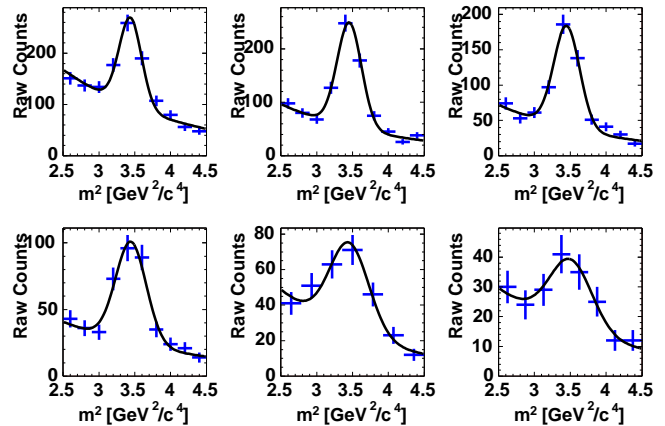


FIG. 1: (color online) Histograms of the mass squared for identified antideuterons in the transverse momentum range $1.1 < p_T < 3.5$ GeV/ c (in 400 MeV/ c increments), with Gaussian fits including an exponential background.

pancy. Corrections are determined by reconstructing single deuterons simulated using GEANT [10] and a detector response model of PHENIX, using the method described in [6]. The track reconstruction efficiency decreases in high multiplicity events because of high detector occupancy. This effect can be slightly larger for slower, heavier particles, due to detector dead times between successive hits. Occupancy effects on reconstruction efficiency ($\approx 83.5\%$ for 0-20% most central events) are evaluated by embedding simulated single particle Monte Carlo events in real events. Since the hadronic interactions of nuclei are not treated by GEANT, a correction needs to be applied to account for the hadronic absorption of d and \bar{d} (including annihilation). The d - and \bar{d} -nucleus cross sections are calculated from parameterizations of the nucleon and anti-nucleon cross sections:

$$\sigma_{d/\bar{d},A} = [\sqrt{\sigma_{N/\bar{N},A}} + \Delta_d]^2 \quad (1)$$

The limited data available on deuteron induced interactions [11] indicate that the term Δ_d is independent of the nuclear mass number A and that $\Delta_d = 3.51 \pm 0.25$ mb $^{1/2}$. The hadronic absorption varies only slightly over the applicable p_T range and is $\approx 10\%$ for d and $\approx 15\%$ for \bar{d} . The background contribution from deuterons knocked out due to the interaction of the produced particles with the beam pipe is estimated using simulations and found to be negligible in the momentum range of our measurement.

Figure 2 shows the corrected d and \bar{d} invariant yields as a function of transverse mass (m_T in the range $1.1 < p_T < 4.3$ GeV/ c , for minimum bias events, and two centrality bins: 0-20% (most central), 20-92% (non-central). The 20-92% centrality bin is dominated by mid-central events, due to larger track multiplicities relative to peripheral events.

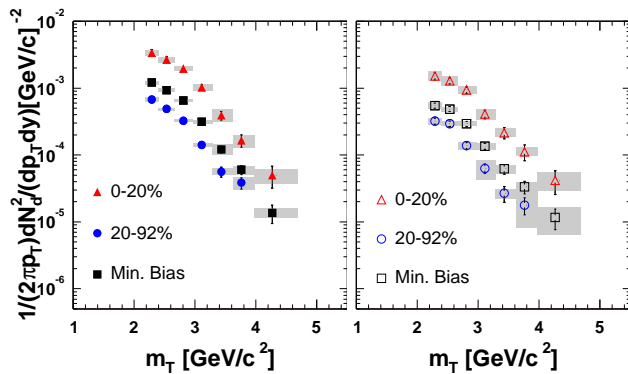


FIG. 2: (color online) Corrected spectra for deuterons (left panel) and anti-deuterons (right panel) for different centralities are plotted vs m_T . Error bars indicate statistical errors and grey bands the systematic errors. Values are plotted at the “true” mean value of m_T of each bin, the extent of which is indicated by the width of the grey bars along x-axis.

TABLE I: The inverse slope parameter T_{eff} obtained from a m_T exponential fit to the spectra along with multiplicity dN/dy and mean transverse momentum $\langle p_T \rangle$ obtained from a Boltzman distribution for different centralities:

T_{eff} [MeV]	Deuterons	Anti-deuterons
Minimum Bias	519 ± 27	512 ± 32
0-20%	536 ± 32	562 ± 51
20-92%	475 ± 29	456 ± 35
dN/dy		
Minimum Bias	$0.0250 \pm_{0.0006(stat.)}^{0.005(sys.)}$	$0.0117 \pm_{0.002(stat.)}^{0.0003(sys.)}$
0-20%	$0.0727 \pm_{0.0141(sys.)}^{0.0022(stat.)}$	$0.0336 \pm_{0.0057(sys.)}^{0.0013(stat.)}$
20-92%	$0.0133 \pm_{0.0029(sys.)}^{0.0004(stat.)}$	$0.0066 \pm_{0.0015(sys.)}^{0.0002(stat.)}$
$\langle p_T \rangle$ [GeV/c]		
Minimum Bias	$1.54 \pm_{0.13(sys.)}^{0.04(stat.)}$	$1.52 \pm_{0.12(sys.)}^{0.05(stat.)}$
0-20%	$1.58 \pm_{0.13(sys.)}^{0.05(stat.)}$	$1.62 \pm_{0.1(sys.)}^{0.07(stat.)}$
20-92%	$1.45 \pm_{0.15(sys.)}^{0.05(stat.)}$	$1.41 \pm_{0.15(sys.)}^{0.06(stat.)}$

Systematic uncertainties have several sources: errors in particle identification, DC-TOF hit match efficiency, the uncertainty in momentum scale, d and \bar{d} hadronic interaction correction, and uncertainty in occupancy corrections. All the systematic uncertainties are added in quadrature, depicted by grey bars in Fig. 2.

The p_T spectra $E d^3 N/d^3 p$ are fitted in the range $1.1 < p_T < 3.5$ GeV/c to an exponential distribution in $m_T = \sqrt{p_T^2 + m^2}$. The inverse slopes (T_{eff}) of the spectra are tabulated in Table I. The deuteron inverse slopes of $T_{eff} = 500$ –520 MeV are considerably higher than the $T_{eff} = 300$ –350 MeV observed for protons [5, 6]. The invariant yields and the average transverse momenta ($\langle p_T \rangle$) are obtained by summing the data over p_T and using a Boltzmann distribution: $\frac{d^2 N}{2\pi m_T dm_T dy} \propto m_T e^{-m_T/T_{eff}}$,

(which gives a slightly better $\chi^2/n.d.f. = 4.8/3$ vs. $\chi^2/n.d.f. = 5.6/3$ for exponential fit) to extrapolate to low m_T regions where we have no data. The extrapolated yields constitute $\approx 42\%$ of our total yields. The rapidity distributions, dN/dy , and the mean transverse momenta, $\langle p_T \rangle$, are compiled in Table I for three different centrality bins. Systematic uncertainties on dN/dy and $\langle p_T \rangle$ are estimated by using an exponential in p_T and a “truncated” Boltzman distribution (assumed flat for $p_T < 1.1$ GeV/c) for alternative extrapolations.

With a binding energy of 2.24 MeV, the deuteron is a very loosely bound state. Thus, it is formed only at a later stage in the collision, most likely after elastic hadronic interactions have ceased; the proton and neutron must be close in space and tightly correlated in velocity to coalesce. As a result, d and \bar{d} yields are a sensitive measure of correlations in phase space and can provide information about the space-time evolution of the system. If deuterons are formed by coalescence of protons and neutrons, the invariant deuteron yield can be related [12] to the primordial nucleon yields by:

$$E_d \frac{d^3 N_d}{d^3 p_d} \Big|_{p_d=2p_p} = B_2 \left(E_p \frac{d^3 N_p}{d^3 p_p} \right)^2 \quad (2)$$

where B_2 is the coalescence parameter, with the subscript implying that two nucleons are involved in the coalescence. The above equation includes an implicit assumption that the ratio of neutrons to protons is unity. The proton and antiproton spectra [6] are corrected for feed-down from Λ and $\bar{\Lambda}$ decays by using a MC simulation tuned to reproduce the particle ratios: (Λ/p and $\bar{\Lambda}/\bar{p}$) measured by PHENIX at 130 GeV [13].

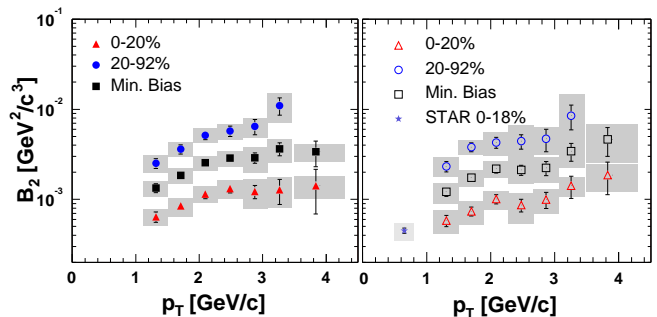


FIG. 3: (color online) Coalescence parameter B_2 vs p_T for deuterons (left panel) and anti-deuterons (right panel). Grey bands indicate the systematic errors. Values are plotted at the “true” mean value of p_T of each bin, the extent of which is indicated by the width of the grey bars along x-axis.

Figure 3 displays the coalescence parameter B_2 as a function of p_T for different centralities. The decreased B_2 in more central collisions implies that in larger sources, the average relative separation between nucleons increases, thus decreasing the probability of formation

of deuterons. We also observe that B_2 increases with p_T . This is consistent with an expanding source because position-momentum correlations lead to a higher coalescence probability at larger p_T . The p_T -dependence of B_2 can also provide information about the density profile of the source as well as the expansion velocity distribution. It has been shown [14] that generally a Gaussian source density profile leads to a constant B_2 with p_T as it gives greater weight to the center of the system, where radial expansion is weakest. This is not supported by our data, which shows a rise in B_2 with p_T .

Thermodynamic models [4] predict that B_2 scales with the inverse of the effective volume V_{eff} ($B_2 \propto 1/V_{eff}$). The d and \bar{d} spectra are affected by radial flow, which concentrates the coalescing protons and neutrons, affecting phase space correlations, thereby limiting the applicability of a simple thermodynamical model to determine an effective source size.

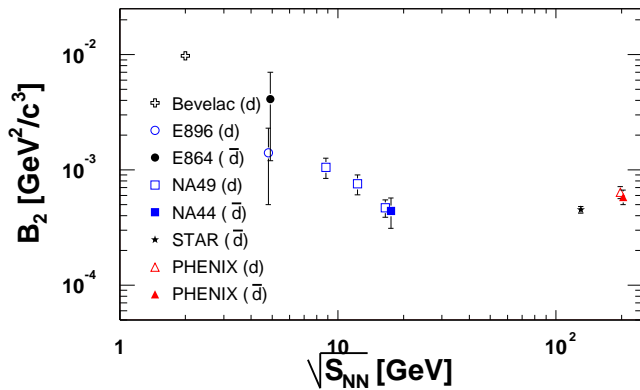


FIG. 4: (color online) Comparison of the coalescence parameter for deuterons and anti-deuterons ($p_T = 1.3$ GeV/c) with other experiments at different values of \sqrt{s} .

Figure 4 compares B_2 for most central collisions to results at lower \sqrt{s} [15, 16, 17, 18, 19, 20]. Note that B_2 is nearly independent of \sqrt{s} , indicating that the source volume does not change appreciably with center-of-mass energy (with the caveat that B_2 varies as a function of p_T , centrality and rapidity). Similar behavior is seen for B_2 for deuterons [18] as a function of \sqrt{s} . This observation is consistent with what has been observed in Bose-Einstein correlation Hanbury-Brown Twiss (HBT) analysis at RHIC [21] for identified particles. The coalescence parameter B_2 for d and \bar{d} , is equal within errors, indicating that nucleons and antinucleons have the same temperature, flow and freeze-out density distributions.

The ratio \bar{n}/n can be estimated from the data based on the thermal chemical model. Assuming thermal and chemical equilibrium, the chemical fugacities are deter-

mined from the particle/anti-particle ratios [14]:

$$\frac{E_A(d^3 N_A/d^3 p_A)}{E_A(\bar{d}^3 N_{\bar{A}}/d^3 p_A)} = \exp\left(\frac{2\mu_A}{T}\right) = \lambda_A^2 \quad (3)$$

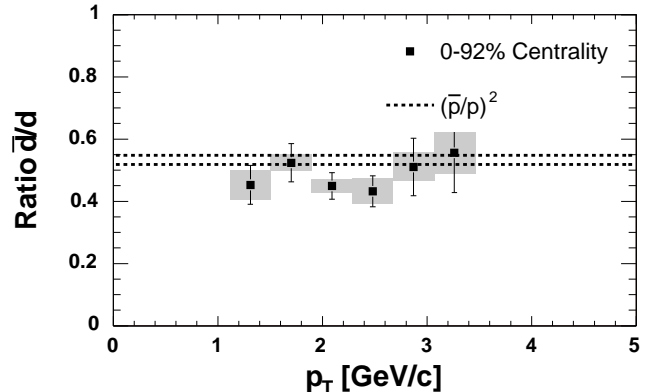


FIG. 5: \bar{d}/d ratio vs. p_T for minimum bias data. The dashed lines represent the square of the measured \bar{p}/p ratio as a function of p_T within uncertainties.

Figure 5 shows that the \bar{d}/d ratio is independent of centrality, and p_T within errors. The average value of \bar{d}/d is 0.47 ± 0.03 , consistent with the square of the ratio $\bar{p}/p = 0.73 \pm 0.01$ [6] within statistical and systematic uncertainties. This is expected if deuterons are formed by coalescence of comoving nucleons and $\bar{p}/p = \bar{n}/n$. Using the ratio p/\bar{p} , the extracted proton fugacity is $\lambda_p = \exp(\mu_p/T) = 1.17 \pm 0.01$. Similarly, using the d/\bar{d} ratio, the extracted deuteron fugacity is $\lambda_d = \exp[(\mu_p + \mu_n)/T] = 1.46 \pm 0.05$. From this, the neutron fugacity can be estimated to be $\lambda_n = \exp(\mu_n/T) = 1.25 \pm 0.04$, which results in $\bar{n}/n = 0.64 \pm 0.04$. These estimates, along with equality of B_2 for d and \bar{d} indicate that, within errors, $\mu_n \geq \mu_p$. This is expected since the entrance Au+Au channel has larger net neutron density than net proton density.

To summarize, the transverse momentum spectra of d and \bar{d} in the range $1.1 < p_T < 4.3$ GeV/c, have been measured at mid-rapidity in Au+Au collisions at $\sqrt{s_{NN}} = 200$ GeV, and are found to be less steeply falling than proton (and antiproton) spectra. This behavior is consistent with a constant (flat) source density profile. The extracted coalescence parameter B_2 increases with p_T , which is indicative of an expanding source. B_2 decreases for more central collisions, consistent with an increasing source size with centrality. The B_2 measured in nucleus-nucleus collisions is independent of $\sqrt{s_{NN}}$ above 12 GeV, consistent with Bose-Einstein correlation measurements of the radii of the source. B_2 is equal within errors for both deuterons and anti-deuterons. From the measurements, it is estimated that $\bar{n}/n = 0.64 \pm 0.04$.

We thank the staff of the Collider-Accelerator and Physics Departments at BNL for their vital contributions. We acknowledge support from the Department of Energy and NSF (U.S.A.), MEXT and JSPS (Japan), CNPq and FAPESP (Brazil), NSFC (China), CNRS-IN2P3 and CEA (France), BMBF, DAAD, and AvH (Germany), OTKA (Hungary), DAE and DST (India), ISF (Israel), KRF and CHEP (Korea), RMIST, RAS, and RMAE, (Russia), VR and KAW (Sweden), U.S. CRDF for the FSU, US-Hungarian NSF-OTKA-MTA, and US-Israel BSF.

* Deceased

† PHENIX Spokesperson:zajc@nevis.columbia.edu

- [1] K. Adcox *et al.*, Phys. Rev. Lett. **86**, 3500 (2001); B. B. Back *et al.*, Phys. Rev. Lett. **88**, 022302 (2002).
- [2] K. Adcox *et al.*, Phys. Rev. Lett. **88**, 242301 (2002); B. B. Back *et al.*, Phys. Rev. **C67**, 021901 (2003); C. Adler *et al.*, Phys. Rev. Lett. **86**, 4778 (2001).
- [3] L. P. Csernai and J. I. Kapusta, Phys. Rep. **131**, 223 (1986).
- [4] A. Z. Mekjian, Phys. Rev. **C17**, 1051 (1978).
- [5] K. Adcox *et al.*, Phys. Rev. **C69**, 024904 (2004);
- [6] S. S. Adler *et al.*, Phys. Rev. **C69**, 034909 (2004).
- [7] K. Adcox *et al.*, Nucl. Instrum. Methods **A499**, 469 (2003) and references therein.
- [8] J. T. Mitchell *et al.*, Nucl. Instrum. Methods **A482**, 491 (2002).
- [9] S. S. Adler *et al.*, Phys. Rev. Lett. **91**, 072301 (2003).
- [10] GEANT 3.21, CERN program library.
- [11] J. Jaros *et al.*, Phys. Rev. **C18**, 1978 (2273); E. O. Abdurakhmanov *et al.*, Z. Phys. **C5**, 1980 (1).
- [12] S. T. Butler and C. A. Pearson, Phys. Rev. **129**, 836 (1963).
- [13] K. Adcox *et al.*, Phys. Rev. Lett. **89**, 092302 (2002).
- [14] R. Scheibl, and U. Heinz, Phys. Rev. **C59**, 1585 (1999); A. Polleri, J. P. Bondorf, and I. N. Mishustin, Phys. Lett. **B419**, 19 (1998).
- [15] S. Wang *et al.*, Phys. Rev. Lett. **74**, 2646 (1995).
- [16] S. Albergo *et al.*, Phys. Rev. **C65**, 034907 (2002).
- [17] T. A. Armstrong *et al.*, Phys. Rev. Lett. **85**, 2685 (2000).
- [18] T. Anticic *et al.*, Phys. Rev. **C69**, 024902 (2004).
- [19] I. G. Bearden *et al.*, Phys. Rev. Lett. **85**, 2681 (2000).
- [20] C. Adler *et al.*, Phys. Rev. Lett. **87**, 262301 (2001).
- [21] K. Adcox *et al.*, Phys. Rev. Lett. **88**, 192302 (2002); C. Adler *et al.*, Phys. Rev. Lett. **87**, 082301 (2001).